

## DISCOVERY OF A 112 MS X-RAY PULSAR IN PUPPIS A: FURTHER EVIDENCE OF NEUTRON STARS WEAKLY MAGNETIZED AT BIRTH

E. V. GOTTHELF & J. P. HALPERN

Columbia Astrophysics Laboratory, Columbia University, New York, NY 10027-6601;  
eric@astro.columbia.edu, jules@astro.columbia.edu

Submitted December 29, 2008

### ABSTRACT

We report the discovery of 112-ms X-ray pulsations from RX J0822–4300, the compact central object (CCO) in the supernova remnant Puppis A, in two archival *Newton X-Ray Multi-Mirror Mission* observations taken in 2001. The sinusoidal light curve has a pulsed fraction of 11% with an abrupt 180° change in phase at 1.2 keV. The observed phase shift and modulation are likely the result of emission from opposing thermal hot spots of distinct temperatures. Phase-resolved spectra reveal an emission feature at  $E_{\text{line}} = 0.8$  keV associated with the cooler region, possibly due to an electron cyclotron resonance effect similar to that seen in the spectrum of the CCO pulsar 1E 1207.4–5209. No change in the spin period of PSR J0821–4300 is detected in 7 months, with a  $2\sigma$  upper limit on the period derivative of  $\dot{P} < 8.3 \times 10^{-15}$ . This implies limits on the spin-down energy loss rate of  $\dot{E} < 2.3 \times 10^{35}$  erg s<sup>-1</sup>, the surface magnetic dipole field strength  $B_s < 9.8 \times 10^{11}$  G, and the spin-down age  $\tau_c > 220$  kyr. The latter is much longer than the SNR age, indicating that PSR J0821–4300 was born spinning near its present period. Its properties are remarkably similar to those of the two other known CCO pulsars, demonstrating the existence of a class of neutron stars born with weak magnetic fields related to a slow original spin. These results are also of importance in understanding the extreme transverse velocity of PSR J0821–4300, favoring the hydrodynamic instability mechanism in the supernova explosion.

*Subject headings:* stars: neutron — pulsars: (RX J0822–4300, PSR J0821–4300, 1E 1207.4–5209, PSR J1210–5226, PSR J1852+0040) — supernova remnants: individual (Puppis A)

### 1. INTRODUCTION

Recent timing studies of central compact objects (CCOs) in supernova remnants (SNRs) have found young neutron stars (NSs) whose spin-down is imperceptible due to a weak dipole magnetic field (Gotthelf & Halpern 2008). More generally, CCOs are defined by their steady, predominantly thermal X-ray emission, lack of optical or radio counterparts, and absence of pulsar wind nebulae (see reviews by Pavlov et al. 2004 and De Luca 2008). Of the six firm members of the CCO class, two are identified explicitly as pulsars, while searches for pulsations from the other CCOs have been unsuccessful. In particular, claims have been made for several candidate spin periods of RX J0822–4300, the CCO in Puppis A (Pavlov et al. 1999; Hui & Becker 2006a), but none has been confirmed.

RX J0822–4300 has long been considered the stellar remnant of the supernova explosion that produced Puppis A, given its central location, lack of an optical counterpart, and hot thermal spectral properties (Petre et al. 1982, 1996). Puppis A itself is an oxygen-rich SNR, similar to Cas A. Its age is estimated as  $3.7 \pm 0.4$  kyr from the proper motion of its oxygen knots (Winkler et al. 1998), and its distance  $d = 2.2 \pm 0.3$  kpc is derived from H I absorption features (Reynoso et al. 2002). More recently, an unusually large transverse velocity of  $\approx 1600$  km s<sup>-1</sup> was measured for RX J0822–4300 (Winkler & Petre 2007; Hui & Becker 2006b), testing proposed mechanisms of natal kick.

In this Letter we present a reanalysis of a pair of timing

observation of RX J0822–4300 acquired with the *Newton X-Ray Multi-Mirror Mission (XMM-Newton)* observatory. We find a highly significant pulsed signal in both data sets that imposes an interesting upper limit on the period derivative. PSR J0821–4300 becomes the third CCO pulsar, with timing and spectral properties similar to those of the two other CCO pulsars, PSR J1852+0040 in Kes 79 (Gotthelf & Halpern 2005; Halpern et al. 2007) and PSR J1210–5226 in PKS 1209–51/52 (Gotthelf & Halpern 2007). We discuss the physical basis for the class of CCO pulsars and how their natal properties differ from radio pulsars and magnetars.

### 2. XMM-NEWTON OBSERVATIONS

Two archival *XMM-Newton* observations of RX J0822–4300 are best suited to search for coherent pulsations. These were obtained on 2001 April 15 and November 8 using the European Photon Imaging Camera (EPIC; Turner et al. 2003) operating in “small-window” mode (4′3″×4′3″ field-of-view). This mode provides 5.7 ms time resolution, allowing a search for even the most rapidly rotating young pulsar. The EPIC pn detector is sensitive to X-rays in the nominal 0.1 – 12 keV range with energy resolution  $\Delta E/E \approx 0.1/\sqrt{E(\text{keV})}$ . The medium filter was used with the target placed at the default EPIC pn focal plane location for a point source. The concurrent EPIC MOS data are not used in this work because of its more limited (2.7 s) time resolution.

We reprocessed the EPIC pn data using the Science Analysis System version SAS 7.0.0 (2006028\_1801) and

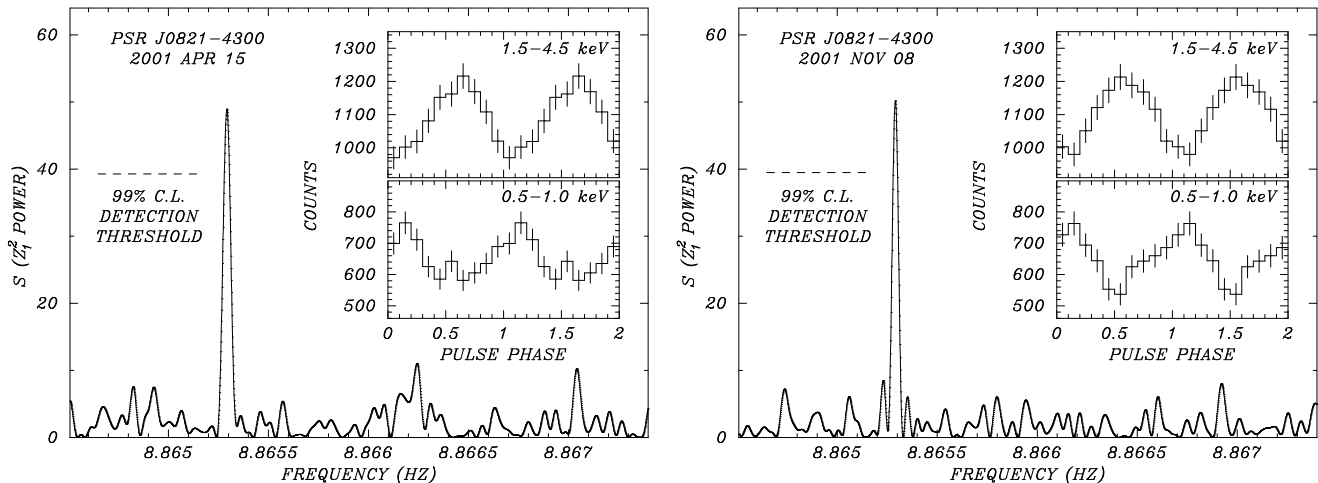


FIG. 1.— Discovery of PSR J0821–4300 in Puppis A using *XMM-Newton* EPIC pn data acquired on 2001 April 15 (left) and November 8 (right). The power spectrum of 1.5 – 4.5 keV photons is extracted from a 30'' radius aperture at the location of RX J0822–4300. The detection threshold for a blind search for a period  $P > 12$  ms is indicated. Inset: Background subtracted pulse profiles of PSR J0821–4300 in two energy bands illustrating the phase shift between the two; the soft photons are extracted from a 18'' radius aperture to minimize the SNR background contamination.

TABLE 1  
*XMM-Newton* TIMING RESULTS FOR PSR J0821–4300

| Epoch<br>(MJD) | Dur.<br>(s) | Bkgn <sup>d</sup> .<br>(s <sup>-1</sup> ) | Source <sup>b</sup><br>(s <sup>-1</sup> ) | Period <sup>c</sup><br>(s) | $f_p$ <sup>d</sup><br>(%) |
|----------------|-------------|---|---|----------------------------|---------------------------|
| 52,014.325     | 22,637      | 0.131(4)                                  | 0.653(8)                                  | 0.112799416(51)            | 11(1)                     |
| 52,221.765     | 22,511      | 0.158(5)                                  | 0.668(8)                                  | 0.112799437(40)            | 11(1)                     |

NOTE. — Statistical uncertainty in the last digit is given in parentheses.

<sup>a</sup> Background rate in the 1.5–4.5 keV band in a  $0'.5 < r < 0'.8$  annular aperture, corrected for dead-time.

<sup>b</sup> Count rate in the 1.5–4.5 keV band in a  $r = 0'.5$  aperture, corrected for dead-time and background.

<sup>c</sup> Period derived from a  $Z_1^2$  test. Uncertainty is  $1\sigma$ , computed by the Monte Carlo method described in Gotthelf et al. (1999).

<sup>d</sup> Observed pulsed fraction, defined as  $f_p \equiv N(\text{pulsed})/N(\text{total})$ , after subtracting background.

screened the photon event lists using the standard criteria. Both observations were uncontaminated by flare events, providing  $\approx 22.5$  ks of good EPIC pn exposure time during each epoch. After taking into account the CCD readout dead-time (29%), this translates to 16 ks of live-time per observation in “small window” mode. Photon arrival times were converted to the solar system barycenter using source coordinates  $08^{\text{h}}21^{\text{m}}57^{\text{s}}.37, -43^{\circ}00'17''.0$  (J2000.0) derived from a contemporaneous *Chandra* observation. In the following analysis we choose a source aperture  $0'.5$  in radius centered on RX J0822–4300 to maximize signal over background, except where otherwise noted. This region encloses  $\geq 80\%$  of the source flux. Count rates and exposure times are presented in Table 1.

### 2.1. Timing Analysis

To search for a pulsed signal, arrival times of photons were initially extracted in the energy band 1.5 – 4.5 keV under the hypothesis that hard X-rays coming from a smaller area might be more strongly pulsed than soft X-rays from the full stellar surface. A  $2^{23}$ -bin Fast Fourier Transform was used. The most significant signal de-

tected was  $P = 112$  ms in both EPIC pn data sets, with no higher harmonics. We constructed a periodogram centered on this signal using the  $Z_1^2$  (Rayleigh) test (Buccheri et al. 1983) and localized the pulsed emission with a peak statistic of  $Z_1^2 = 48.94$  and  $Z_1^2 = 50.20$  for the 2001 April and November observations, respectively. These statistics correspond to 99.991% and 99.995% confidence, respectively, after allowing for the number of independent trials ( $2\Delta T_{\text{span}}/P_{\text{min}}$ ) in a blind search for  $P_{\text{min}} > 12$  ms, the Nyquist limit. The timing results are summarized in Table 1.

The periods derived from the  $Z_1^2$  test are statistically identical. The periodogram derived from each data set is shown in Figure 1 along with the pulse profile folded at the best period. With a single coherent fold using both data sets, a total power of  $Z_1^2 = 95.98$  is recovered without the need for a period derivative. This corresponds to a negligible probability of chance occurrence. The formal result is  $\dot{P} = (1.2 \pm 3.6) \times 10^{-15} \text{ s s}^{-1}$ . The uncertainty is  $1\sigma$  and is computed by propagating the uncertainties on the individual period measurements. From the  $2\sigma$  upper-limit of  $\dot{P} < 8.3 \times 10^{-15} \text{ s s}^{-1}$  we constrain the spin-down power of PSR J0821–4300 to  $\dot{E} \equiv 4\pi^2 I \dot{P} / P^3 < 2.3 \times 10^{35} \text{ erg s}^{-1}$ , the surface dipole magnetic field strength to  $B_s = 3.2 \times 10^{19} \sqrt{P \dot{P}} < 9.8 \times 10^{11} \text{ G}$ , and the characteristic age to  $\tau_c \equiv P/2\dot{P} > 220 \text{ kyr}$ .

The background-subtracted pulsed fraction is  $11 \pm 1\%$  for both observations. The pulsed fraction is defined here as  $f_p \equiv N(\text{pulsed})/N(\text{total})$ , where we choose the minimum of the folded light curves as the unpulsed level. The pulse shape is evidently unchanged between observations, suggesting a stable underlying emission process. No other significant signal is detected in either data set. In particular, we examined the two weaker candidate signals reported by Hui & Becker (2006a) from these observations. Although we see these peaks, neither is statistically significant or repeatable between the two observations. We also analyzed all archival X-ray data sets that might yield detections of PSR J0821–4300 and further constrain its timing parameters, but none proved

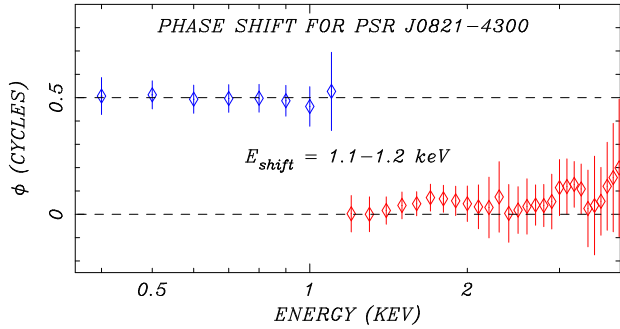


FIG. 2.— Pulse phase as a function of energy for PSR J0821–4300. The phases and errors are determined by cross-correlating energy-selected folded light curves with a master template. The phase is computed for overlapping 0.5 keV wide energy slices incremented in 0.1 keV steps. Phase zero is defined as the minimum of the modulation as shown in Figure 1. The result using the April 15 data set is shown; the November 8 data yields an equivalent result. Both show a half cycle phase shift at  $E_{\text{shift}} = 1.1 - 1.2$  keV.

sensitive enough.

A search for the signal in the softer energy band reveals that the pulse is indeed present, below 1.0 keV, but shifted in phase by half a cycle relative to the hard pulse. Figure 2 shows that the phase shift is remarkably abrupt, with a half cycle step ( $\Delta\phi = 0.5$ ) at an energy of 1.1 – 1.2 keV. The location of the shift is unresolved to better than  $\sim 0.25$  keV, limited by the counting statistics and the EPIC pn energy resolution of  $\sim 0.1$  keV at 1 keV. This shift effectively cancels the signal in a full-spectrum search.

## 2.2. Phase-Resolved Spectroscopy

Hui & Becker (2006a) performed a comprehensive spectral analysis of the *XMM-Newton* data on RX J0822–4300, showing that a two-component fit is necessary. They preferred a double blackbody model, which is also compatible with our expectation that surface thermal emission dominates over any other source of X-rays from CCOs. We can investigate the cause of the phase shift in the pulse profiles by examining pulse phase-resolved spectra and searching for features that may be phase-dependent. In particular, we extracted two spectra, one in the phase band centered on the pulse peak found in the harder energy band ( $\phi = 0.5$ ), as shown in Figure 1, and the other centered on the phase band found for the softer emission ( $\phi = 0.0$ ). Each spectrum covers a phase interval 0.4 cycles and is referred to herein as the hard and soft phase spectra.

We combined data from both observations and grouped the two phase resolved spectra with a minimum of 100 counts per channel. These were fitted to the double blackbody model in the 0.4 – 4.0 keV energy range. We find that both spectra can be fitted with the same component temperatures, with phase-dependent normalization. The fitted spectra are shown in Figure 3 and the best fit parameters are listed in Table 2. For the soft phase there is clear evidence of positive residuals from the continuum model in the 0.7 – 0.9 keV range. This is well modeled by the addition of a Gaussian emission line of  $E_{\text{line}} = 0.79 \pm 0.02$  keV with an equivalent width of  $W \approx 55$  eV. Comparing a fit without and with the line feature results in a change from  $\chi^2 = 69.41$  to  $\chi^2 = 53.45$ , for 70 and 67 degrees-of-freedom, re-

TABLE 2  
PHASE RESOLVED *XMM-Newton* SPECTRAL RESULTS FOR PSR J0821–4300

| Parameter                           | Soft Phase             | Hard Phase           |
|-------------------------------------|------------------------|----------------------|
| $N_{\text{H}}$ ( $\text{cm}^{-2}$ ) | $4.8 \pm 0.06$         | (Linked)             |
| $kT_1$ (keV)                        | $0.21^{+0.05}_{-0.02}$ | (Linked)             |
| $kT_2$ (keV)                        | $0.42^{+0.04}_{-0.3}$  | (Linked)             |
| $L_1(BB)$ ( $\text{erg s}^{-1}$ )   | $4.1 \times 10^{33}$   | $3.3 \times 10^{33}$ |
| $L_2(BB)$ ( $\text{erg s}^{-1}$ )   | $2.5 \times 10^{33}$   | $3.2 \times 10^{33}$ |
| $A_1(BB)$ ( $\text{cm}^2$ )         | $2.1 \times 10^{12}$   | $1.7 \times 10^{12}$ |
| $A_2(BB)$ ( $\text{cm}^2$ )         | $7.8 \times 10^{10}$   | $9.9 \times 10^{10}$ |
| Gaussian Line Component             |                        |                      |
| $E_{\text{line}}$ (keV)             | $0.79 \pm 0.03$        | (Linked)             |
| $\sigma_{\text{line}}$ (eV)         | $53^{+33}_{-22}$       | (Linked)             |
| $W$ (eV)                            | $\approx 55$           | $\lesssim 9$         |
| $\chi^2$ (dof)                      | 125.6 (153)            |                      |

NOTE. — Spectral fits in the 0.4 – 4 keV energy band, for two phase regions, 0.4 cycles wide, one centered on the pulse peak found in the softer energy band (“soft phase”) and the other centered on phase found in the harder energy band (“hard phase”). All errors are at the 90% confidence level.

spectively. For the hard-phase spectrum, the continuum model provides a satisfactory fit without the need for an added line component ( $W \lesssim 9$  eV).

Given the excellent fits to the double blackbody model the most natural explanation of the emission from PSR J0821–4300 is that of two discrete “hot spots” on the surface of the neutron star, corresponding to the two blackbody temperatures and areas. As the star rotates, the hard emission dominates over the soft component when the hotter side is facing the viewer, while half a cycle later, the soft emission dominates as the harder emission is now (partially) eclipsed by the star. Based on their phase relationship, evidently  $180^\circ$ , the two spots are on opposite sides of the NS.

Several measurements favor this explanation: 1) both the soft and hard phase spectra can be fitted to a double blackbody model with the same component temperatures, but phase dependent normalizations, 2) the phase shift energy ( $E_{\text{shift}} = 1.1 - 1.2$  keV) is in agreement with the cross-over energy between blackbody components for the above best fit model ( $E_{\text{cross}} = 1.16$  keV; cf. Figure 2 and Figure 3), 3) for this model fit, the magnitude of the pulse modulation is consistent with the change of the derived areas for both the soft and hard phase spectra (see Table 2).

In this picture, the geometry is strongly constrained. The small modulation requires that the spin axis be nearly aligned with the line-of-sight. Furthermore, the hot spot axis must be nearly perpendicular to the spin axis since both temperature components are evident throughout the rotation phase. Future modeling of the observed spectrum and light curves will allow us to test this hypothesis, of opposed thermal hot-spots for PSR J0821–4300, and quantify the hot-spot and viewing geometries (e.g., Perna & Gotthelf 2008). This study should also provide important constraints on the previously allowed spectral models (Hui & Becker 2006a) of the pulsar.

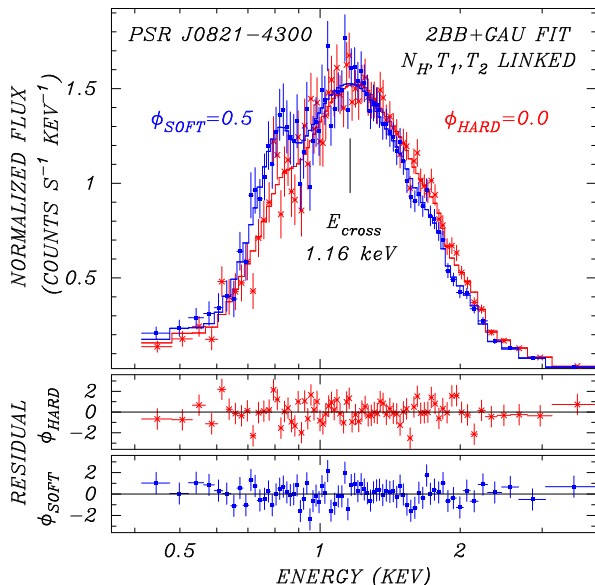


FIG. 3.— Phase-resolved spectra from the summed *XMM-Newton* observations of PSR J0821–4300. The two spectra correspond to two phase regions, 0.4 cycles wide, one centered on the pulse peak found in the softer energy band (“ $\phi_{SOFT}$ ”) and the other centered on the peak found in the harder energy band (“ $\phi_{HARD}$ ”). In each case, a double blackbody model plus Gaussian emission line is fitted with the parameters given in Table 2; the column density and temperatures are linked. The cross-over energy,  $E_{cross} = 1.16$  keV, of the two spectra, is shown. Residuals of the data from the model for the two spectra are shown in the lower panels; the soft phase data require a significant line component at  $E_{line} = 0.79$  keV.

### 3. DISCUSSION

#### 3.1. Physical Basis of the CCO Class

In the dipole spin-down formalism, the  $2\sigma$  lower limit of  $\tau_c > 220$  kyr on the characteristic age of PSR J0821–4300, in combination with its true (SNR) age of  $T = 3.7$  kyr, implies that its initial spin period  $P_0 = P\sqrt{1 - T/\tau_c}$  is identical to its current period  $P = 112$  ms to  $< 1\%$  accuracy. Thus, PSR J0821–4300 becomes the third CCO whose initial spin period is known to be large, and whose surface dipole magnetic field strength,  $B_s < 9.8 \times 10^{11}$  G, is smaller than those of the canonical young radio pulsars. In comparison, the upper limits on  $B_s$  from timing of PSR J1210–5226 (Gotthelf & Halpern 2007) and PSR J1852+0040 (Halpern et al. 2007) are  $< 3.3 \times 10^{11}$  G and  $< 1.5 \times 10^{11}$  G, respectively.

PSR J0821–4300 is virtually a twin of the 105 ms pulsar PSR J1852+0040 in Kes 79 which, however, is  $\sim 80\%$  pulsed. In contrast, the weak ( $f_p \approx 11\%$ ) pulse of PSR J0821–4300 is more similar to the light curve of the 424 ms pulsar PSR J1210–5226. The latter is most notable for the prominent cyclotron absorption lines in its soft X-ray spectrum. For PSR J0821–4300, the likely detection of a weak emission line is reminiscent of the energy dependence of the pulse phase in PSR J1210–5226 (Pavlov et al. 2002; De Luca et al. 2004), which suggests that electron cyclotron resonance processes may be affecting its pulse shape. The surface  $B$ -field strength of PSR J1210–5226 is estimated to be  $\approx 8 \times 10^{10}$  G from its absorption features (Bignami et al. 2003), in particular, the cyclotron fundamental at 0.7 keV, and the magnetic field of PSR J0821–4300 may be similar.

The physics of the CCO class, evidently characterized

by weak magnetic field and slow, original spin, may lie in the turbulent dynamo that generates the magnetic field. The strength of the dynamo depends on the rotation rate of the proto-neutron star (Thompson & Duncan 1993; Bonanno et al. 2006), so the magnetic field strength is inversely correlated with the initial period.

#### 3.2. Spin-Kick Mechanisms

*Chandra* proper motion measurements of RX J0822–4300 reveal an extraordinarily large transverse velocity ( $1570 \pm 240 d_2 \text{ km s}^{-1}$ , Winkler & Petre 2007;  $1122 \pm 360 d_{2.2} \text{ km s}^{-1}$ , Hui & Becker 2006b). As discussed by Winkler & Petre (2007), this high velocity restricts the possible models for NS kicks, of which there are three broad categories (see Lai 2001 and Wang et al. 2006). The discovery of the spin parameters of PSR J0821–4300 now allows us to eliminate two of these models: 1) the magnetic-induced asymmetric neutrino emission model requires a magnetic field of  $> 10^{15}$  G (Lai 2001) and can only produce velocities  $< 250 \text{ km s}^{-1}$ , and 2) the electromagnetic rocket effect (Harrison & Tademaru 1975; Lai 2001) needs an initial spin period  $< 1$  ms to achieve the velocity of PSR J0821–4300. Therefore, the third model, that of hydrodynamic instability during the explosion (Burrows et al. 2007), emerges as the most likely explanation for large NS kicks. This is consistent with a highly asymmetric explosion, as indicated for Puppis A, wherein the momentum of the oxygen knots match the momentum of RX J0822–4300, but in the opposite direction (Winkler & Petre 2007).

Interestingly, the hydrodynamic mechanism is the one mechanism of the three candidate theories that does *not* lead naturally to alignment between the spin axis and the direction of proper motion that is observed in the slowly moving Crab ( $v_t \approx 120 \text{ km s}^{-1}$ ) and Vela ( $v_t \approx 60 \text{ km s}^{-1}$ ) pulsars, and is statistically evident in larger samples of pulsars (Johnston et al. 2005; Ng & Romani 2007). If the spin of PSR J0821–4300 were aligned with its velocity, which is nearly in the plane of the sky, then we would have expected to see a large rotational modulation from any surface hot spot. On the contrary, if the slow initial spin period of PSR J0821–4300 is longer than the duration of the kick mechanism, the impulse of the asymmetric kick could have been expended in one direction rather than being averaged out by rotation. Thus, the long spin period of PSR J0821–4300 allows its spin axis and velocity vector to be misaligned. This is consistent with our model for the weak modulation, where the spin axis is close to the line-of-sight, nearly perpendicular to the velocity vector, as is allowed for a large kick from the hydrodynamic mechanism.

### 4. CONCLUSIONS AND FUTURE WORK

The discovery of PSR J0821–4300 advances the argument, reviewed by Gotthelf & Halpern (2008), that slow original spin and weak magnetic field constitute the physical basis of the CCO class. There may even be a causal connection between slow natal spin and weak magnetic field through a turbulent dynamo that creates the magnetic field. The next step is a dedicated timing study of PSR J0821–4300 to determine whether it is spinning down steadily, and to measure its period derivative and

dipole magnetic field. An alternative possibility that it is accreting from a fallback disk (Halpern et al. 2007) can also be tested by detailed timing. Similar studies are underway for the other CCO pulsars.

We predict that most if not all of the remaining CCOs will turn out to be weakly magnetized pulsars with  $P \gtrsim 0.1$  s. These may include the CCO in Cassiopeia A, and possibly an as-yet unseen NS in SN 1987A. In the absence of spin parameters, is difficult to discriminate between a low magnetic field CCO and a quiescent magnetar on the basis of an X-ray spectrum alone, as these classes have similar spectral properties. Before the CCO pulsars were known, both Cas A and SN 1987A were hypothesized to host magnetars. However, the recent retraction (Kim et al. 2008; Dwek & Arendt 2008) of claimed evidence from the *Spitzer Space Telescope* for an historic

SGR-like outburst in Cas A (Krause et al. 2005) leaves a weakly magnetized NS as the most compelling model for that youngest of known CCOs. In the case of Cas A, we must allow for the possibility that an energy-dependent phase shift similar to PSR J0821–4300 makes it difficult to detect pulsations. We are searching for similar effects in all CCOs.

This investigation is based on observations obtained with *XMM-Newton*, an ESA science mission with instruments and contributions directly funded by ESA Member States and NASA. This work is was made possible by NASA XMM grant NNX08AX67X, which provided critical hardware support.

## REFERENCES

- Bignami, G. F., Caraveo, P. A., De Luca, A., & Mereghetti, S. 2003, *Nature*, 423, 725
- Bonanno, A., Urpin, V., & Belvedere, G. 2006, *A&A*, 451, 1049
- Buccheri, R., et al. 1983, *A&A*, 128, 245
- Burrows, A., Livne, E., Dessart, L., Ott, C. D., & Murphy, J. 2007, *ApJ*, 655, 416
- De Luca, A. 2008, in *AIP Conf. Proc. 983, 40 Years of Pulsars: Millisecond Pulsars, Magnetars, and More*, ed C. Bassa, Z. Wang, A. Cumming, & V. M. Kaspi (New York: AIP), 311
- De Luca, A., Mereghetti, S., Caraveo, P. A., Moroni, M., Mignani, R. P., & Bignami, G. F. 2004, *A&A*, 418, 625
- Dwek, E., & Arendt, R. G. 2008, *ApJ*, 685, 976
- Gotthelf, E. V. & Halpern, J. P. 2007, *ApJ*, 664, L35
- . 2008, in *AIP Conf. Proc. 983, 40 Years of Pulsars: Millisecond Pulsars, Magnetars, and More*, ed C. Bassa, Z. Wang, A. Cumming, & V. M. Kaspi (New York: AIP), 320
- Gotthelf, E. V., Halpern, J. P., & Seward, F. D. 2005, *ApJ*, 627, 390
- Gotthelf, E. V., Vasisht, G., Dotani, T. 1999, *ApJ*, 522, L49
- Halpern, J. P., & Gotthelf, E. V., Camilo, F., & Seward, F. D. 2007, *ApJ*, 665, 1304
- Harrison, E. R., & Tademaru, E. 1975, *ApJ*, 201, 447
- Hui, C. Y., & Becker, W. 2006a, *A&A*, 454, 543
- . 2006b, *A&A*, 457, L33
- Johnston, S., Hobbs, G., Vigeland, S., Kramer, M., Weisberg, J. M., & Lyne, A. G. 2005, *MNRAS*, 364, 1397
- Kim, Y., Rieke, G. H., Krause, O., Misselt, K., Indebetouw, R., & Johnson, K. E. 2008, *ApJ*, 678, 287
- Krause, O., et al. 2005, *Science*, 308, 1604
- Lai, D. 2001, in *Physics of Neutron Star Interiors*, ed. D. Blaschke, N. K. Glendenning, & A. Sedrakian (Berlin: Springer), 424
- Lai, D., Chernoff, D. F., & Cordes, J. M. 2001, *ApJ*, 549, 1111
- Ng, C.-Y., & Romani, R. W. 2007, *ApJ*, 660, 1357
- Pavlov, G. G., Sanwal, D., & Teter, M. A. 2004, in *Young Neutron Stars and their Environment*, IAU Symp. 218, ed. F. Camilo & B. M. Gaensler (San Francisco: ASP), 239
- Pavlov, G. G., Zavlin, Sanwal, D., & Trümper, J. 2002, *ApJ*, 569, L95
- Pavlov, G. G., Zavlin, & Trümper, J. 1999, *ApJ*, 511, L45
- Petre, R., Becker, C. M., & Winkler, P. F. 1996, *ApJ*, 465, L43
- Perna, R. & Gotthelf, E. V. 2008, *ApJ*, 681, 522
- Petre, R., Canizares, C. R., Kriss, G. A., & Winkler, P. F. 1982, *ApJ*, 258, 22
- Reynoso, E.M., Dubner, G.M., Gross, W.M., & Arnal, E.M. 1995, *AJ*, 110, 318
- Thompson, C., & Duncan, R. C. 1993, *ApJ*, 408, 194
- Turner, M. J. L., Briel, U. G., Ferrando, P., Griffiths, R. G., & Villa, G. E. 2003, *SPIE*, 4851, 169
- Wang, C., Lai, D., & Han, J. L. 2006, *ApJ*, 639, 1007
- Winkler, P.F., & Petre, R. 2007, *ApJ*, 670, 635